Geophysical Journal International

Geophys. J. Int. (2014) **199,** 1286–1302 doi: 10.1093/gji/ggu330
GJI Marine geosciences and applied geophysics

Structure and deformation of the Kermadec forearc in response to subduction of the Pacific oceanic plate

M. J. Funnell,[1] C. Peirce,[1] W. R. Stratford,[1] M. Paulatto,[2,4] A. B. Watts[2] and I. Grevemeyer[3]

[1]*Department of Earth Sciences, Durham University, South Road, Durham, DH*1 3*LE, UK. E-mail: matthew.funnell2@durham.ac.uk*
[2]*Department of Earth Sciences, University of Oxford, Oxford, OX*1 3*PR, UK*
[3]*GEOMAR, Helmholtz Centre of Ocean Research, D-*24148 *Kiel, Germany*
[4]*Géoazur, Bât* 4, 250 *Rue Albert Einstein, Les Lucioles* 1, *Sophia-Antipolis, F-*06560 *Valbonne, France*

Accepted 2014 August 27. Received 2014 August 18; in original form 2014 June 30

Downloaded from http://gji.oxfordjournals.org/ at Durham University Library on September 30, 2014

SUMMARY

The Tonga-Kermadec forearc is deforming in response to on-going subduction of the Pacific Plate beneath the Indo-Australian Plate. Previous research has focussed on the structural development of the forearc where large bathymetric features such as the Hikurangi Plateau and Louisville Ridge seamount chain are being subducted. Consequently, knowledge of the 'background' forearc in regions of normal plate convergence is limited. We report on an ∼250-km-long multichannel seismic reflection profile that was shot perpendicular to the Tonga-Kermadec trench at ∼28°S to determine the lateral and temporal variations in the structure, stratigraphy and deformation of the Kermadec forearc resulting solely from Pacific Plate subduction.

Interpretation of the seismic profile, in conjunction with regional swath bathymetry data, shows that the Pacific Plate exhibits horst and graben structures that accommodate bending-induced extensional stresses, generated as the trenchward dip of the crust increases. Trench infill is also much thicker than expected at 1 km which, we propose, results from increased sediment flux into and along the trench. Pervasive normal faulting of the mid-trench slope most likely accommodates the majority of the observed forearc extension in response to basal subduction erosion, and a structural high is located between the mid- and upper-trench slopes. We interpret this high as representing a dense and most likely structurally robust region of crust lying beneath this region.

Sediment of the upper-trench slope documents depositional hiatuses and on-going uplift of the arc. Strong along-arc currents appear to erode the Kermadec volcanic arc and distribute this sediment to the surrounding basins, while currents over the forearc redistribute deposits as sediment waves. Minor uplift of the transitional Kermadec forearc, observed just to the north of the profile, appears to relate to an underlying structural trend as well as subduction of the Louisville Ridge seamount chain 250 km to the north. Relative uplift of the Kermadec arc is observed from changes in the tilt of upper-trench slope deposits and extensional faulting of the basement immediately surrounding the Louisville Ridge.

Key words: Controlled source seismology; Subduction zone processes; Dynamics and mechanics of faulting; Fractures and faults.

1 INTRODUCTION

Subduction of the Pacific Plate occurs along 2700 km of the Tonga-Kermadec trench (Fig. 1). This classic example of an intra-oceanic, non-accretionary and erosional convergent plate margin exhibits the fastest rates of convergence and the most linear trench–forearc complex of the global subduction system (Brodie & Hatherton 1958; Dickinson & Seely 1979; Bevis *et al.* 1995). Since the Pacific Plate began to subduct beneath the Indo-Australian Plate in the Mid-Eocene, the Tonga-Kermadec forearc and arc have developed into the multicomponent system seen today (Hawkins *et al.* 1984; Clift *et al.* 1998). The Kermadec trench and forearc, which comprise the southern section of this subduction system, are separated from the Tonga trench to the north, and the Hikurangi trench to the south, by subduction of the Louisville Ridge seamount chain (LRSC) and Hikurangi Plateau, respectively (Ballance *et al.* 1989; Davy 1992).

Forearcs evolve in response to changes in the rate, angle and obliquity of subduction as well as the strength and roughness of the

© The Author 2014. Published by Oxford University Press on behalf of The Royal Astronomical Society.

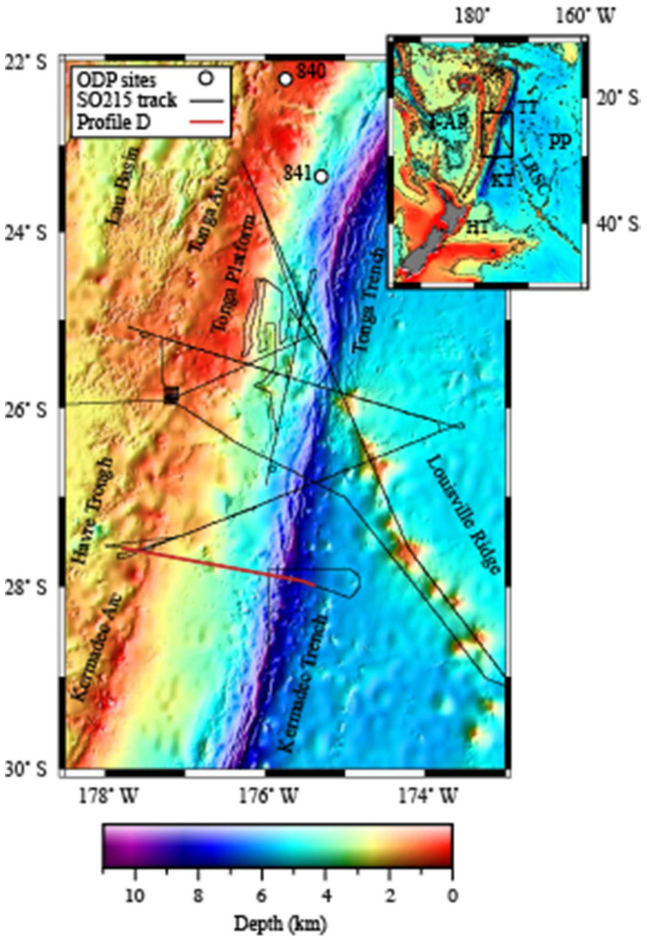

Figure 1. Bathymetry map of the Tonga-Kermadec subduction system. The study area, indicated by the black box on the inset map, stretches from 22 to 30°S and 173 to 178.5°W. The inset map shows that although the Pacific Plate (PP) subducts beneath the Indo-Australian Plate (I-AP) along the length of this subduction zone, the Kermadec trench (KT) is separated from the Tonga and Hikurangi trenches (TT and HT) by the collision of the Louisville Ridge seamount chain (LRSC) and Hikurangi Plateau, respectively. Profile D (red line) is an MCS transect through the Kermadec trench-forearc system at ~28°S, located to image the structural and stratigraphic development of the forearc. The study location map is repeated in Figs 2–6 to indicate the extent of MCS and bathymetry data displayed within each figure, and to locate each figure within the regional context.

subducting plate (Dickinson & Seely 1979; von Huene & Scholl 1991). Variations in these characteristics often manifest themselves as changes in the dominant stress regime (Bonnardot *et al.* 2007), and the rate of frontal and basal subduction erosion of the overriding plate (Clift & Vannucchi 2004; von Huene *et al.* 2004). The LRSC and Hikurangi Plateau are thickened and buoyant regions of oceanic lithosphere, whose subduction is observed to have had a significant effect on the structural development of the forearc of the overriding plate (Collot & Davy 1998; Davy & Collot 2000; Contreras-Reyes *et al.* 2011; Stratford *et al.* 2014). Despite numerous investigations of the subduction and forearc deformation processes to the north and south, the structure of the Kermadec trench and forearc are constrained only by spatially restricted swath bathymetry and low resolution, single channel seismic reflection data (Karig 1970; Dickinson & Seely 1979; Katz 1981; Herzer *et al.* 1984). As a result, the subsurface structure of the Kermadec trench and forearc remains poorly understood, and little is known of the sedimentation and deformation processes that have influenced forearc development since subduction initiation.

In 2011, wide-angle seismic refraction and multichannel seismic (MCS) reflection data were acquired, together with Parasound, gravity, magnetic, swath bathymetry and backscatter data, along profiles crossing the Tonga-Kermadec trench–arc system (Peirce & Watts 2011). This study uses data acquired along Profile D, which crosses the trench at ~28°S, to better understand Kermadec forearc structure, principal deformation styles and their lateral variations between 26.5°S and 30°S by: (i) imaging the stratigraphy and structures of the subducting and overriding plates; (ii) determining how sediments are transported and deposited across the different regions of the trench–forearc system, and how this has changed over time; (iii) resolving structural features in the MCS, Parasound and swath bathymetry data to understand along-profile forearc deformation and (iv) relating these sedimentary and deformation processes to trends and variations in the bathymetric characteristics of the outer- and inner-trench slopes of the Tonga-Kermadec subduction system. A discussion of the changes in forearc deformation and structures caused by seamount subduction at the Tonga-Kermadec subduction system can be found in Stratford *et al.* (2014).

2 GEOLOGICAL SETTING

The tectonic history of the Tonga-Kermadec subduction system is both multistage and complex (Parson *et al.* 1992). Although the present-day volcanic arcs originated closer to their respective trenches (Clift & MacLeod 1999), they have supplied volcaniclastic material to the surrounding basins since the Eocene (Sutherland 1995). Subduction of the Pacific Plate initiated in the middle Eocene (~44 Ma—McDougall 1994; Bloomer *et al.* 1995), causing the inner forearc slope to rise ~1 km, and the trench to depress to its current depth (Ballance *et al.* 1989; Parson *et al.* 1992). The abundance of volcaniclastic material, dated as late Miocene in age, implies the presence of a single volcanic chain before this time (Ballance *et al.* 1989). This single-arc system remained stable until rifting of the Lau Basin began at ~7.8 Ma (Clift 1994; Ballance *et al.* 1999), and the Havre Trough opened ~5 Ma (Malahoff *et al.* 1982; Clift *et al.* 1994). Initiation of rifting in these backarc basins coincides with a peak in the generation of volcaniclastic material. An ~2 Myr regional hiatus in sedimentation followed this increased volcanic output (Clift 1994; Ballance *et al.* 1999). Tectonic erosion of the overriding plate has progressively extended and depressed the Tonga forearc by ~280 per cent and ~6 km, respectively since the Miocene (Clift *et al.* 1994; MacLeod 1994). These changes, relative to the effectively static depth of the volcanic arc with time, cause the forearc to rotate towards the trench (Clift & MacLeod 1999).

The Pacific and Indo-Australian plates converge at rates of up to 164–249 mm yr^{-1} along the Tonga-Kermadec subduction system (Bevis *et al.* 1995). An 020° trending trench axis, with a mean depth of ~8 km (Ballance *et al.* 1989), delimits the zone where old (~80 Ma) and dense Pacific Plate is thrust beneath the Indo-Australian Plate (Lonsdale 1988; Fig. 1). Along this subduction zone the crust and mantle of the Pacific oceanic lithosphere is most likely hydrated through new bend-related faults that are generated across the outer rise (Ranero *et al.* 2003). Fast rates of convergence and the hydration of this cold and brittle oceanic lithosphere cause the Tonga-Kermadec subduction system to be one of the most seismically and volcanically active in the global subduction system (Bevis *et al.* 1995; Grevemeyer *et al.* 2005).

Downloaded from http://gji.oxfordjournals.org/ at Durham University Library on September 30, 2014

Trench-parallel normal faults form in the poorly sedimented underthrusting (downgoing) plate as it passes over the outer rise and bends towards the trench (Lonsdale 1986; MacLeod 1994). Ballance *et al.* (1989) and MacLeod (1994) proposed that arc-derived volcaniclastic sediments, transported via submarine canyons, dominate the fill of the graben structures as they subduct. This process is observed along the sediment-starved convergent margin off northern Chile, and is supplemented by the addition of crustal material disaggregated from the forearc basement (von Huene & Ranero 2003; Ranero *et al.* 2006; Maksymowicz *et al.* 2012). Although the lack of sediments on the subducting plate prevents the formation of an accretionary wedge along the northern Chile and Tonga-Kermadec subduction zones, the abundance of forearc-derived material along the northern Chile margin generates a frontal prism under a compressive regime (Shreve & Cloos 1986; von Huene & Ranero 2003).

Currently, the structure and morphology of the Tonga-Kermadec trench–forearc system varies significantly along its length (Fig. 1). A steeply dipping (10–24°) and highly irregular basement with little sediment cover characterizes the inner-trench slope (Karig 1970; Ballance *et al.* 1999). Poor sedimentation of the trench and inner slope is a consequence of reduced sediment transport, which results from sediment ponding in basins located higher up on the forearc (Dickinson & Seely 1979). Mid-slope terraces, for example, act as effective sediment traps and are located along the length of the Tonga-Kermadec forearc at ~5–6 km water depth (e.g. Brodie & Hatherton 1958; Karig 1970; Ballance *et al.* 1999). Extension in the lower- and middle-trench slopes has been inferred from the presence of normal faults observed in cores at ODP Site 841 (Fig. 1, MacLeod 1994) and low seismic velocity regions modelled from wide-angle seismic refraction data (Contreras-Reyes *et al.* 2011; Stratford *et al.* 2014). This extensional zone is associated with the presence of an ~2000-km-long scarp, more prominent in the Tonga forearc than the Kermadec forearc, located ~60 km behind the trench (Contreras-Reyes *et al.* 2011). von Huene *et al.* (2004) hypothesize that such extension, and thus subsidence, of the lower- and mid-trench slopes results from the hydrofracturing and subsequent removal of basal material from the overthrusting plate.

Single channel seismic reflection data from Karig (1970) indicate that the Kermadec forearc is dominated by a thick sedimentary succession, which is divided into two clear units by a bright reflection event. The Karig (1970) data failed to image the internal structure of the deposits of the upper forearc, and so they were described as acoustically transparent. Clift *et al.* (1994) recognized full Bouma sequences (Bouma 1962) in cores at ODP site 840, located on the Tonga Platform (Fig. 1), and speculated that turbidite flows dominate sedimentation on the upper-trench slopes.

Formed by volcanism related to the subduction of thinly sedimented crust (Ballance *et al.* 1989; Castillo *et al.* 2009), the Tonga and Kermadec arcs lie ~200 km west of their respective trenches. These volcanic chains are elevated significantly above the surrounding forearc and backarc, allowing distribution of volcaniclastic material to the adjacent basins (Brodie & Hatherton 1958; Karig 1970). These volcanic arcs are continually being uplifted (Ballance *et al.* 1989). Strike-slip and normal fault systems found on the western slope of the Tonga and Kermadec arcs reflect their oblique angle of subduction (Bonnardot *et al.* 2007), while on-going extension in the Lau Basin and Havre Trough causes increasing separation of the arcs from their respective backarcs (Delteil *et al.* 2002).

There are two major changes in tectonic regime along the length of the subduction system. At ~26°S, an observed reduction in shallow seismicity coincides with the collision of the LRSC and the Tonga-Kermadec trench (Haberman *et al.* 1986). Geochemical anomaly data obtained from lavas located at ~22°S on the Tonga Arc, north of the present-day LRSC collision zone, indicate that subduction of the LRSC initiated at least 7 Ma (Timm *et al.* 2013). The most northwesterly and currently subducting seamount of the volcanic chain (which are commonly ~2 km high and 10–40 km in diameter) causes a bathymetric discontinuity in the trench and at the lower-trench slope (Lonsdale 1988). This discontinuity divides the Tonga trench–forearc system to the north from the Kermadec trench–forearc system in the south (Karig 1970; Pelletier & Dupont 1990), and causes segmentation into the different tectonic regimes (Bonnardot *et al.* 2007). The oblique strike (335°) of the 4300-km-long seamount chain and the oblique plate convergence, cause the point of collision to migrate southward at ~180 mm yr^{-1} (Ballance *et al.* 1989). Thus, the Tonga forearc has experienced the effects of LRSC subduction, whereas the Kermadec forearc has not.

Subduction of the LRSC elevates and then lowers the overriding forearc, causing it to be faulted and thus weakened (Clift & MacLeod 1999). This process is thought to constitute the majority of subduction erosion that is observed at this boundary, surpassing that which normally occurs at the front and base of the overriding plate as Pacific oceanic crust is subducted (von Huene & Scholl 1991; Clift & Vannucchi 2004). The effect of this increased and accelerated tectonic erosion is manifest in the significant loss of forearc material over a short period of time (estimated to be ~80 km^3—Clift & MacLeod 1999), and observed as a substantial thinning and shortening of the forearc, which results in an increase in slope gradient (Ballance *et al.* 1989).

The second major tectonic boundary occurs at 32°S along the Kermadec trench, where Karig (1970) first noted an anomalous increase in trench depth to the south. There is a coincident 10 km westward step in the forearc (Pelletier & Dupont 1990), together with significant increases in the depth and narrowing of the mid-slope terrace (Ballance *et al.* 1999). An increase in the dip angle of the subducting plate is thought to cause these variations that, in turn, progressively rotate the forearc trenchward (Ballance *et al.* 1999). This 32°S boundary is also associated with the partitioning on the western slope of the Kermadec forearc of strike-slip and normal faulting, to the north and south, respectively (Bonnardot *et al.* 2007).

3 DATA ACQUISITION AND PROCESSING

The ~250-km-long MCS profile traversing the Kermadec subduction system south of the LRSC collision zone was acquired from the 2011 April 29 to May 1 as part of *R/V Sonne* cruise SO215 (Peirce & Watts 2011), which followed on from the **To**nga **T**hrust earthquake **A**sperity at **L**ouisville Ridge (TOTAL) project (Grevemeyer & Flüh 2008). This MCS line, Profile D in Peirce & Watts (2011), was located to study 'background' processes and structures associated with the subduction of Pacific oceanic lithosphere uninfluenced by LRSC subduction. The profile runs perpendicular to the trench–arc system, from ~50 km to the east of the trench to 35 km west of the present-day Kermadec arc (Fig. 2). Gravity, magnetic, Parasound and multibeam bathymetry data were acquired contemporaneously.

The seismic source consisted of a 10 G-gun array, with a combined volume of 4400 in^3 (68 l), which was towed at a depth of 7.5 m and fired at a pressure of 2400 psi (170 bar). Shots were fired every 30 s which, at the ship speed of ~4.5 kn, resulted in an ~70 m interval between shots. The acquisition system also included a 3 km

Downloaded from http://gji.oxfordjournals.org/ at Durham University Library on September 30, 2014

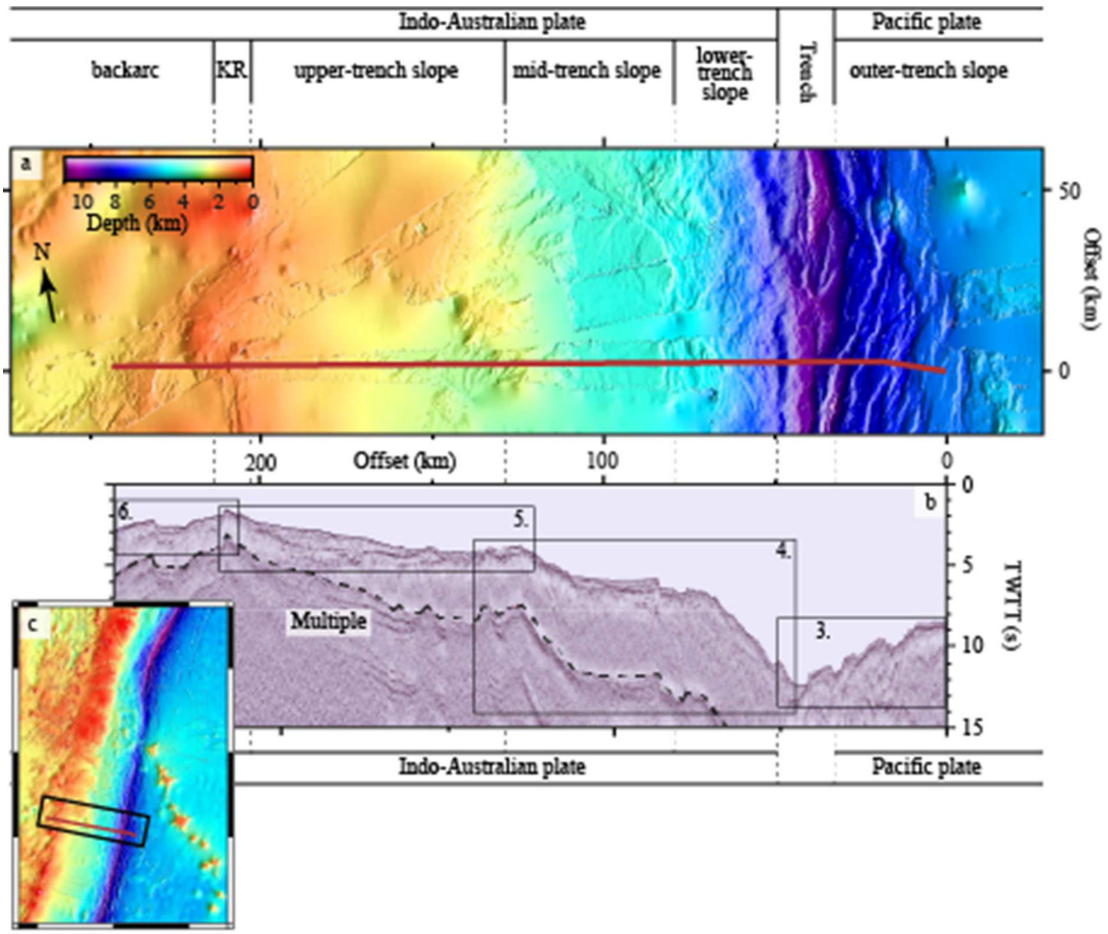

Figure 2. Major structural units of the Tonga-Kermadec trench-forearc system (top) characterized by (a) the swath bathymetry and (b) MCS data acquired along Profile D. KR is the Kermadec ridge. Profile D is marked by a red line in (a) and (c). Boxes and numbers indicate the extents of Figs 3–6 to aid correlation of specific features within the context of the entire seismic profile. A dashed line indicates the water column multiple. Offsets along all subsequent seismic sections and bathymetry maps increase westward and northward from the origin of Profile D, as shown in (a). (c) Extent of the bathymetry and MCS data (black box and red line respectively) displayed in this figure, shown relative to the study area.

multichannel streamer, comprising 240 channels at 12.5 m group interval, towed at 10 m depth. The data set collected consists of 29 s long traces, recorded at a sampling rate of 1 ms. Each common midpoint (CMP), separated by 6.25 m, has a maximum theoretical fold of ∼20.

Initial analysis of the MCS data indicated a low signal-to-noise ratio, as might be expected of a subduction zone where the seabed is rough and scattering, and the subsurface geology is complex. By grouping the CMPs into 25 m bins, the fold was increased from ∼20 to ∼80 and significantly improved the signal-to-noise ratio, whilst also reducing variations in CMP spacing caused by shooting the profile at specific shot times rather than on intrashot distance. Increased CMP bin sizes also improve the resolution of the MCS data at depth. Although increasing the bin size is undertaken at the expense of optimum horizontal resolution, interpretation of the final stacked section is not affected because the seafloor and subsurface structures are still significantly larger than the increased CMP spacing.

A simple processing scheme was applied comprising velocity analysis, stacking, post-stack deconvolution, bandpass filtering and migration. Detailed velocity analysis, required to ensure that lateral changes in seafloor relief and subseabed velocity variations are correctly represented in the velocity model, was conducted using a combination of semblance, constant velocity stacks and gathers, and undertaken at intervals of 25 CMPs (fewer in more structurally complex regions). Well-constrained velocity picks were possible throughout the sedimentary units. However, the lack of subbasement (crustal) reflections resulted in a simple velocity gradient being applied below the basement. The assumption of a velocity gradient from the top of the basement to the bottom of the seismic section is inconsequential to later interpretation given the absence of observable subbasement primary reflections. Post-stack deconvolution sharpened the wavelet, and effectively removed a short-path multiple delayed ∼220 ms behind the primary reflection. The deconvolution operator was designed using the primary reflection generated by a horizontal and planar region of seabed overlying a unit of flat-lying sediments. A Butterworth filter (bandpass range: 3–10–100–120 Hz) reduced noise outside of the useful data bandwidth; in particular the low frequency, high amplitude wave noise recorded during rougher sea states. The application of a post-stack, constant velocity (1500 m s^{-1}) Kirchhoff migration reduced the appearance of high amplitude diffraction tails generated by the rough seabed. For display purposes, a mute was applied before the primary seabed reflection, and a long time-gate (2000 ms) automatic gain control (AGC) equalized reflection amplitudes along each trace. The MCS data were not time-to-depth converted due to a lack of actual velocity control other than stacking velocities derived from velocity analysis.

Downloaded from http://gji.oxfordjournals.org/ at Durham University Library on September 30, 2014

High-resolution, shallow subseabed imaging data, collected by the shipboard Atlas Parasound P70, were recorded in ~800 ms windows around the seabed. The recording delay was determined by the swath-derived seabed depth, and stored in the SEG-Y headers. Application of a bandpass filter (2.0–2.5–5.5–6.0 kHz) around the dominant signal frequency of 4 kHz reduced noise, and an AGC of 200 ms improved the appearance for display.

A shipboard SIMRAD EM120 multibeam echo sounding system acquired swath bathymetry data throughout the cruise. Processing of the raw data in MB-System included the flagging of data that had deviated from the local median depth by more than 100 m between beams to enable the removal of bathymetric artefacts introduced during acquisition (Caress & Chayes 1996). The cleaned swath bathymetry and backscatter amplitude data were gridded at 50 m intervals before being merged with existing ship-track data to produce an updated, but still sparse, high-resolution map of the seafloor (Fig. 2). These data were then combined with the General Bathymetric Chart of the Oceans (GEBCO-IOC *et al.* 2003) 30 arcsec grid to provide a more complete regional bathymetric map (Fig. 1).

4 INTERPRETATIVE DISCUSSION

Profile D crosses the Kermadec trench at ~28°S (Fig. 1). At this location, processes associated with the subduction of background Pacific oceanic lithosphere should cause the majority of deformation to the Kermadec forearc. In this section, a detailed interpretation of Profile D (Fig. 2) focuses on the structure and stratigraphy of the major units that comprise the Kermadec trench–arc system. This interpretation is then related to Parasound subseabed images and bathymetry maps to draw conclusions about the on-going deformation throughout the background Kermadec trench region. Fig. 2 shows where each of the following figures, which display specific structural regions and features in detail, are located along Profile D. For ease of correlation, all 'depth' and 'thickness' estimates are reported in two-way traveltime (TWTT). Comparisons of these data with Profile A (Peirce & Watts 2011), which images structures and deformation of the Tonga forearc associated with LRSC subduction, are made in Stratford *et al.* (2014).

4.1 General overview of Profile D

The subducting Pacific oceanic plate is characterized by a thin cover of sediment (<0.2 s TWTT thick) and extensive normal faulting. This old oceanic plate, imaged along the easternmost 50 km of Profile D, enters the trench at a water depth of 12.4 s TWTT (~9300 m). Despite being clearly imaged across the ~5 km wide and sediment-filled (up to 1 s TWTT) trench, the seismic reflection response of the downgoing plate reduces significantly as it begins to underthrust beneath the overthrusting Indo-Australian Plate.

The overthrusting Indo-Australian Plate can be subdivided into five major structural units: the lower-trench slope; mid-trench slope; upper-trench slope with associated forearc basin; the Kermadec arc and the Lau-Havre backarc basin (Fig. 2). For 20 km west of the trench, the irregular morphology of the lower-trench slope shallows steeply (~10°) to 6.7 s TWTT (~5000 m) water depth. A decrease in bathymetric gradient and thickening of the sedimentary sequence characterizes the transition from the lower- to mid-trench slope at ~6 s TWTT. Further west, the mid-trench slope consists of a 25-km-wide plateau and adjacent slope. The structure of the basement of the mid-trench slope is not concordant with seabed features, implying a complex structural history. The slope to the west of the plateau shallows by 2.1 s TWTT to form a forearc structural high. From here the upper-trench slope rises for ~70 km into the arc. The forearc basin, situated on the upper-trench slope, is characterized by sediments that reach their thickest (~2 s TWTT) towards the centre of the slope region (175–185 km offset). At the western limit of the upper-trench slope (~210 km offset), the forearc shallows to a water depth of 1.45 s TWTT (~1100 m). Although no active volcano is present at the latitude of Profile D, this section of the Kermadec Ridge is coincident with an active volcanic arc (Karig 1970). Profile D images ~30 km of the backarc slope, which displays sediment cover averaging 1 s TWTT thick.

4.2 Pacific oceanic plate

Fig. 3 displays the extent of the Pacific Plate imaged along Profile D (~50 km). The downgoing oceanic lithosphere exhibits uniform but thin sediment cover (~0.2 s TWTT—see Fig. 3a inset). Seabed and intra-sediment reflections, concordant with those of the top of the crust, indicate steady and laterally consistent deposition. These deposits are likely to be dominated by pelagic sediments that have accumulated since the crust formed ~80 Ma; however, they may also include thin successions of volcaniclastic sediments introduced by the LRSC and Kermadec arc volcanic centres, such as those observed at ODP site 204 (Burns *et al.* 1973).

On Profile D, the lateral continuity of the reflections that characterize the Pacific Plate is limited by normal faults of a range of scales (from <0.05 to 0.8 s TWTT offset—Fig. 3b). Lonsdale (1986) and Aubouin (1989) note that these extensional structures form when oceanic crust passes over the flexural bulge of the subducting plate, giving rise to an ~80-km-wide fault zone. Fault offsets and the dip angle of the plate increase to ~2 km and ~5°, respectively with proximity to the trench (Figs 3b and e). These faults form in response to the dominant formation stress, which is a bend-induced tension (Caldwell *et al.* 1976), and grow as the tension intensifies (to several kilobars) effectively relaxing the stresses applied to the crust and uppermost mantle of the subducting oceanic plate in regions of high curvature (Watts *et al.* 1980).

Swath bathymetry data from the region indicate that the horst and graben structures on the downgoing plate trend between 010° and 030° (Fig. 3e). This roughly trench-parallel fabric extends along the length of the Tonga-Kermadec subduction system, and is broken into 50–200-km-long segments, approximately 5–15 km in width. These horst and graben characteristics are similar to those observed at other examples of bend-related faulting from around the Pacific, such as offshore Nicaragua (Ranero *et al.* 2003; Grevemeyer *et al.* 2005). The trench-parallel trend of these bend faults is perpendicular to the fabric of formation for Pacific oceanic lithosphere at this latitude (Billen & Stock 2000), supporting the hypothesis that new faults will form parallel to the trench in oceanic lithosphere if the fabric of formation is >25° from the trend of the trench (Billen *et al.* 2007). Approximately 150 km south of the LRSC collision zone, deformation of the subducting plate appears to partition. South of this point, minor variations in the fault trend and structure show no coherency. However, to the north, the vertical offset of these faulting structures reduces considerably, causing the trench axis to shallow by ~4.5 km towards the current point of collision with the LRSC (Pontoise *et al.* 1986). For example, compare seabed depths at <75 and >225 km offset perpendicular to Profile D in Fig. 3(e). Thus, we define the subduction of purely background Pacific oceanic plate

Downloaded from http://gji.oxfordjournals.org/ at Durham University Library on September 30, 2014

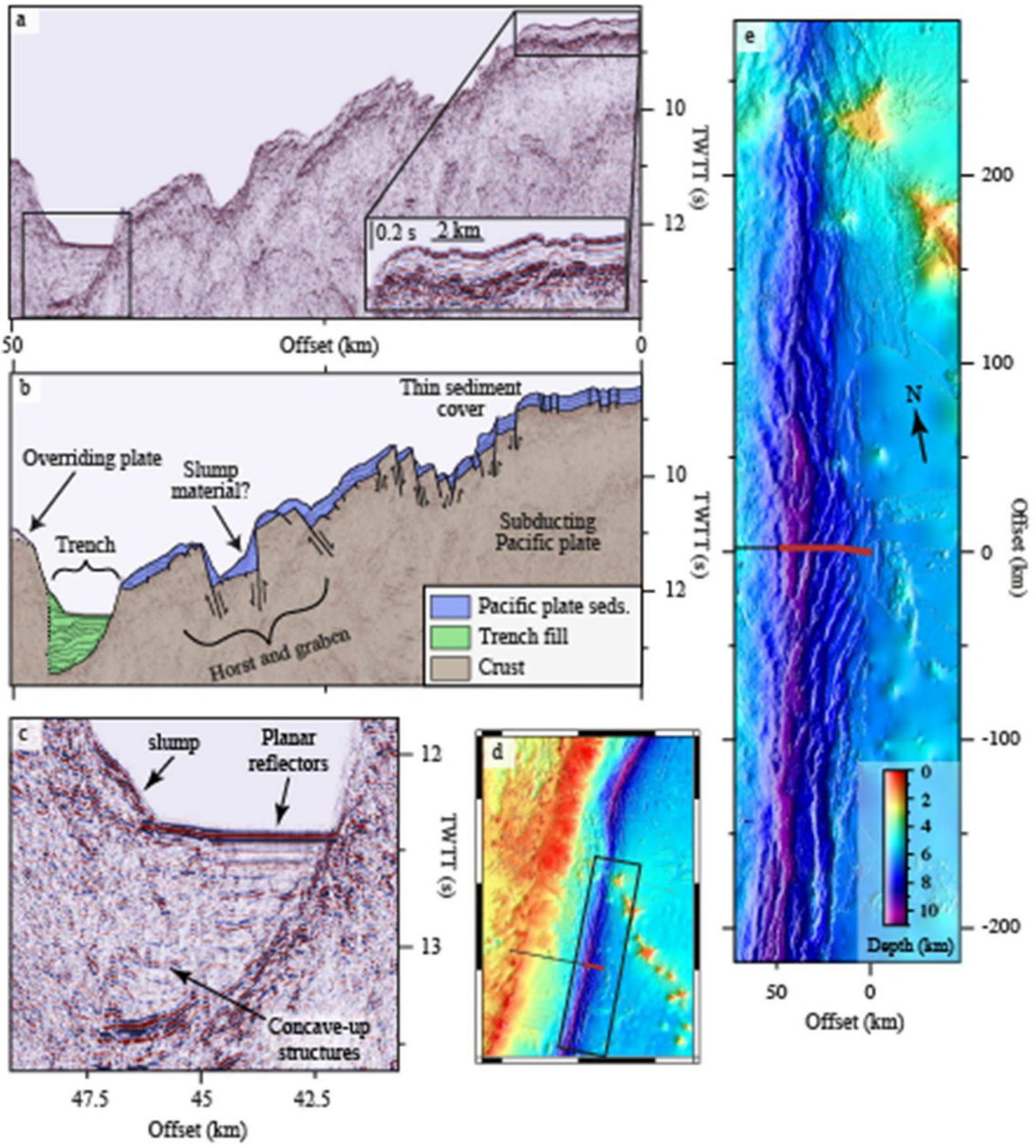

Figure 3. (a) Processed seismic section of the subducting Pacific Plate and Kermadec trench, with the inset section highlighting the nature of sedimentary reflections on the downgoing plate. Black outline box indicates the region of MCS data shown in Fig. 3(c). (b) Interpreted seismic section. Inset key indicates the different seismostratigraphic units. (c) Detailed image of the sediment-filled trench. Note the reflection geometry varies laterally through the trench fill, from horizontal and planar in the east to concave-up structures in the west. (d) Extent of the bathymetry and MCS data (black box and red line respectively) displayed in this figure, shown relative to the study area. (e) Combined swath and satellite-derived bathymetry map of the subducting plate and trench around Profile D.

as that which occurs further than 150 km south of the present-day LRSC–trench collision point, and note that north of this boundary, the bathymetry of the trench axis gradually shallows until the LRSC is reached.

4.3 Trench fill

Along Profile D, the sediment fill of the 5-km-wide trench exhibits reflection characteristics that vary significantly over the lateral extent of the trench (shown in detail in Fig. 3c). Towards the east, reflections are relatively horizontal and planar, displaying slight onlap onto the subducting crust. However, further west these same reflections adopt vertically stacked concave-up structures (~2 km wide), and are covered by a wedge of sediment that thickens with proximity to the overriding plate. This high-angle wedge demonstrates steep eastward-dipping reflections, which suggests that it represents a sediment slump originating on the inner-trench slope. Trench fill is thought to be dominated by undeformed forearc-derived sediment and sediment from the subducting plate, particularly in the vicinity of the sediment-filled LRSC flexural moat (Ballance *et al.* 1989; von Huene & Ranero 2003). Although the presence of a slump indicates that forearc-derived sediment accounts for some of the fill of the trench along this profile, there is no apparent evidence for other mechanisms of trench fill.

Downloaded from http://gji.oxfordjournals.org/ at Durham University Library on September 30, 2014

The Tonga and Kermadec trenches are widely considered to be sediment starved, and thus only exhibit minor sediment fill of <400 m (Karig 1970; Clift & Vannucchi 2004; Contreras-Reyes *et al.* 2011). Profile D indicates a 1 s TWTT thick trench fill that, assuming a sediment velocity of 2000 m s^{-1}, equates to ~1 km of sediment. This excess fill may be caused by a greater than expected flux of forearc-derived material directly into the trench axis (e.g. Ballance *et al.* 1989), or by increased sediment transportation along the trench axis (e.g. Völker *et al.* 2013), which is most likely directed southwards along the dominant bathymetric gradient, or a combination of both. A similar disparity in the thickness of trench fill is observed across the intersection of the Juan Fernández Ridge (JFR) with the central Chile margin (Laursen *et al.* 2002). The JFR acts as a barrier to the transportation of sediments north along the central Chile Trench, generating a 2.5-km-thick sediment accumulation south of the intersection whilst leaving an ~200-m-thick deposit to the north (von Huene *et al.* 1997; Laursen *et al.* 2002). Although the variation in trench-fill across the ridge–trench collision zone is considerably smaller across the LRSC, trench shallowing of up to 4.5 km around this intersection (see Fig. 3e) most likely prevents significant sediment transportation between the Tonga and Kermadec Trenches through a similar mechanism. The vertical succession of bowl-shaped reflections close to the overriding plate along Profile D suggests that a deep-water channel, ~2 km wide, existed along the trench that was capable of redistributing sediments, including volcaniclastic material from the LRSC flexural moat. The presence of such a channel-forming and thus erosive bottom current could also explain the absence of other features, such as older slumps, in the trench. Despite this, channel structures are not well defined in the swath bathymetry data collected along the Kermadec trench (Fig. 3e). Channels are, though, observed in a number of trenches around the Pacific (e.g. Lewis 1994; Völker *et al.* 2013), although commonly at shallower depths than the Kermadec trench, which suggests that their apparent absence here is most likely a result of the complex seabed geometry and reduced resolution of the bathymetry at depth.

4.4 Lower-trench slope

Despite being imaged for 20 km of Profile D, the structure of the lower-trench slope is poorly resolved (Fig. 4). Minimal sediment cover (<0.1 s TWTT) causes the bathymetry of the slope to roughly mirror the irregular surface of the basement (as seen in Karig 1970). The lack of observed sediments, relative to the substantial infill of the trench, is most likely the result of the ~10° gradient that encourages sediment to cascade down the slope and into the trench. Although a frontal prism may be expected at this convergent margin because of the abundant forearc-derived sediments (von Huene *et al.* 2004), the steep angle of slope and lack of actual velocity constraint prevents imaging.

The basement of the lower-trench slope is thought to be highly deformed (Karig 1970; Dickinson & Seely 1979). The proposed extensive fracturing of this region, inferred from reduced seismic wave velocities through the inner trench slope of the Tonga forearc, supports this hypothesis (Contreras-Reyes *et al.* 2011). Although a lack of observable faults and offsets along Profile D itself prevents any definitive conclusions being drawn on the Kermadec lower-trench slope structure, the irregular surface geometry and steeply dipping nature of the slope along the entire Kermadec forearc alone suggests that it has been highly deformed (Figs 4b and d).

4.5 Mid-trench slope

Major faulting of the seabed and a significant reduction in bathymetric gradient ~30 km west of the trench, delimit the region where the lower- and mid-trench slopes merge (Fig. 4d). Along Profile D, the mid-trench slope is dominated by an ~25-km-wide terrace. This plateau is the surface expression of a sedimentary wedge that increases in thickness to the east (up to ~2 s TWTT), and is bounded by a 750-m-offset, trenchward-dipping normal fault ~80 km along the profile (Fig. 4b). High acoustic backscatter amplitudes along the fault, relative to those from the plateau, suggest that this is the most recently formed of many large-offset (~0.5 s TWTT) and basement-cutting normal faults observed in the MCS data (Fig. 4b). Across this fault, the seabed is downthrown to the east; however, where this fault intersects with the crust, the basement reflector exhibits downthrow to the west. The disparity between the seabed and basement structure around this fault suggests slip reversal along an older fault, which is further supported by the divergence of reflectors with proximity to the fault in the lower part of the sedimentary wedge. This fault reversal, along with older faults that created the uplifted basement block observed beneath the sediment wedge to the west, suggests that faulting is migrating eastward across the mid-trench slope. The prevalence of these basement-cutting and apparently migrating normal faults are facilitating the gradual collapse of the lower- and mid-trench slopes into the trench, which is evidence that the model of subduction erosion proposed by von Huene *et al.* (2004) may be occurring here.

Significant extension and basin rotation are observed at ODP site 841 and in the MCS data collected on the Tonga mid-trench slope, near the present day LRSC collision zone (Parson *et al.* 1992; Clift *et al.* 1994; Stratford *et al.* 2014). Clift & MacLeod (1999) use varying rates of subsidence and tilting to infer that the majority of subduction erosion at this location can be attributed to LRSC subduction. Pervasive, but minor, extensional faulting of the mid-slope plateau is observed in both the MCS and Parasound data (Figs 4a and b inset, respectively), and appears to be in response to the slight arcward rotation of the eastern end of the wedge following recent fault activation.

In contrast to the region proximal to the LRSC (e.g. Clift *et al.* 1994), the slight extension and negligible rotation observed along Profile D is evidence of the temporally consistent tectonic erosion caused by the subduction of background Pacific crust at ~28°S. Clift & MacLeod (1999) calculate that <1.5 km Myr^{-1} of frontal tectonic erosion occurs along the Tonga-Kermadec subduction system during this steady-state period. The >100-km-long arcuate normal fault, observed in the swath bathymetry and backscatter data acquired around Profile D, is similar to and as well defined as a similar structure over 250 km further south. To the north of the background subduction zone, the mid-trench slope extensional features are shorter, less well defined, and thus appear to be more deformed. Subduction of seamounts, as Ballance *et al.* (1989) suggest, is most likely to have caused these north–south lateral variations in the characteristics of the deformation of the inner-trench slope.

The steep trenchward dip of the basement beneath the mid-trench plateau results in the sedimentary wedge thinning before abruptly transitioning ~70 km west of the trench into the flanks of a forearc structural high. The across-slope MCS data indicate that a series of basement-cutting normal faults are overlain by <1 s TWTT of poorly resolved sedimentary units (Fig. 4b). This slope is clearly defined as a region of high amplitude backscatter and steep slope angles of ~6° (Figs 4d and d inset), which suggest that older

Downloaded from http://gji.oxfordjournals.org/ at Durham University Library on September 30, 2014

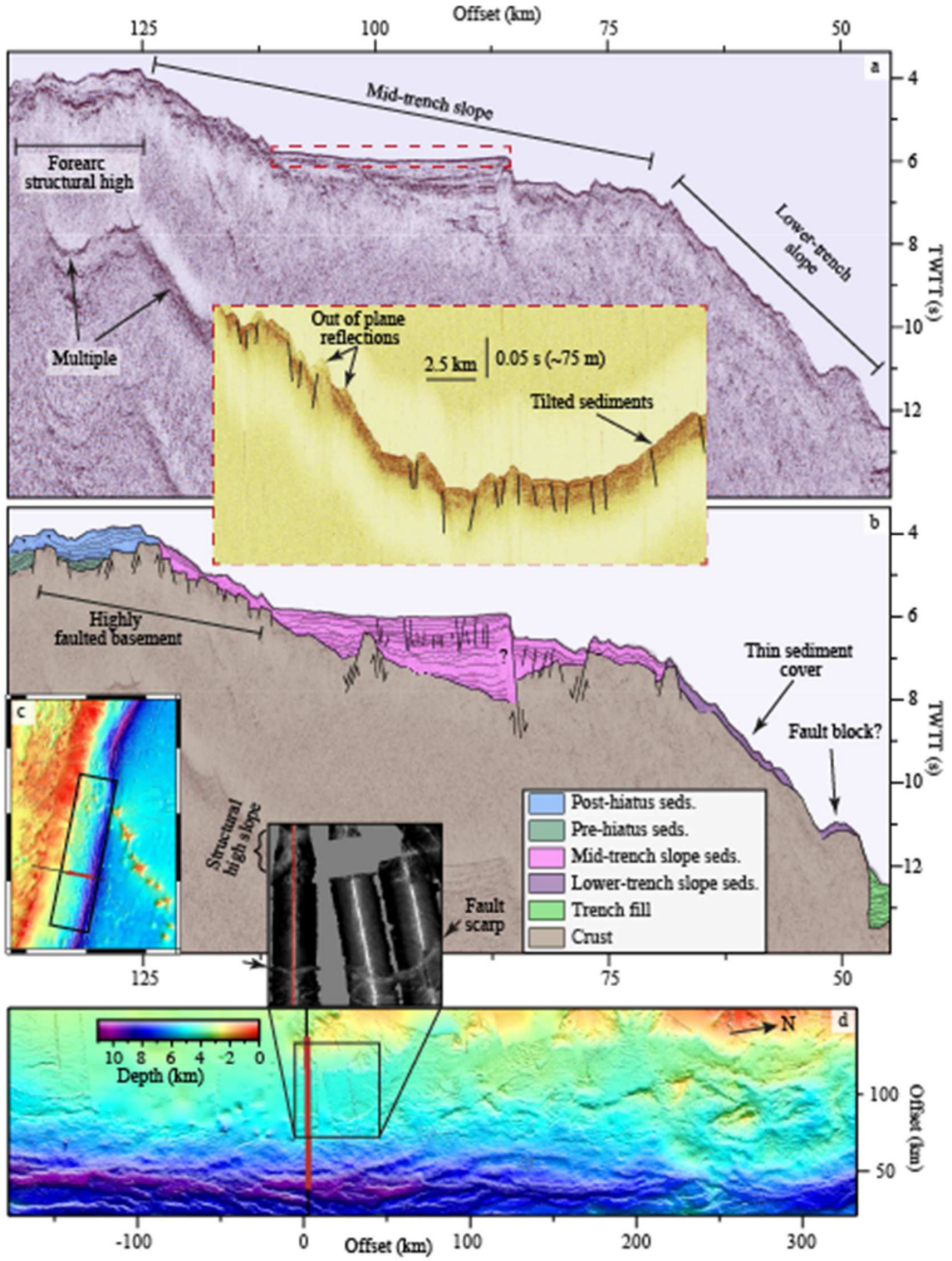

Figure 4. (a) Annotated seismic reflection image of the lower and mid-trench slopes of the overriding Pacific Plate. The onset of the water column multiple is indicated by arrows. Dashed red box indicates the extent of the inset Parasound data. (b) Interpretation of the features in (a), with inset key to indicate the different seismostratigraphic units. (c) Extent of the bathymetry and MCS data (black box and red line, respectively) displayed in this figure, shown relative to the study area. (d) Swath bathymetry map of the lower- and mid-trench regions, highlighting lateral changes in seabed structure. The zoom-in box highlights a recently formed fault surface, and the forearc structural high and its flanks, with their relatively high backscatter amplitudes (lighter regions).

sediments have been exposed as a result of a fault-generated gradient and the subsequent dominance of an erosive regime. Similar backscatter amplitudes, basement faulting and internal deformation of sedimentary deposits are associated with the juxtaposing forearc structural high that is uplifted relative to the mid-trench slope and the eastern extent of the upper-trench slope (Figs 4b and 5b). Whether this feature is caused by active uplift of the structural high or subsidence of the surrounding trench slopes, its presence suggests

Downloaded from http://gji.oxfordjournals.org/ at Durham University Library on September 30, 2014

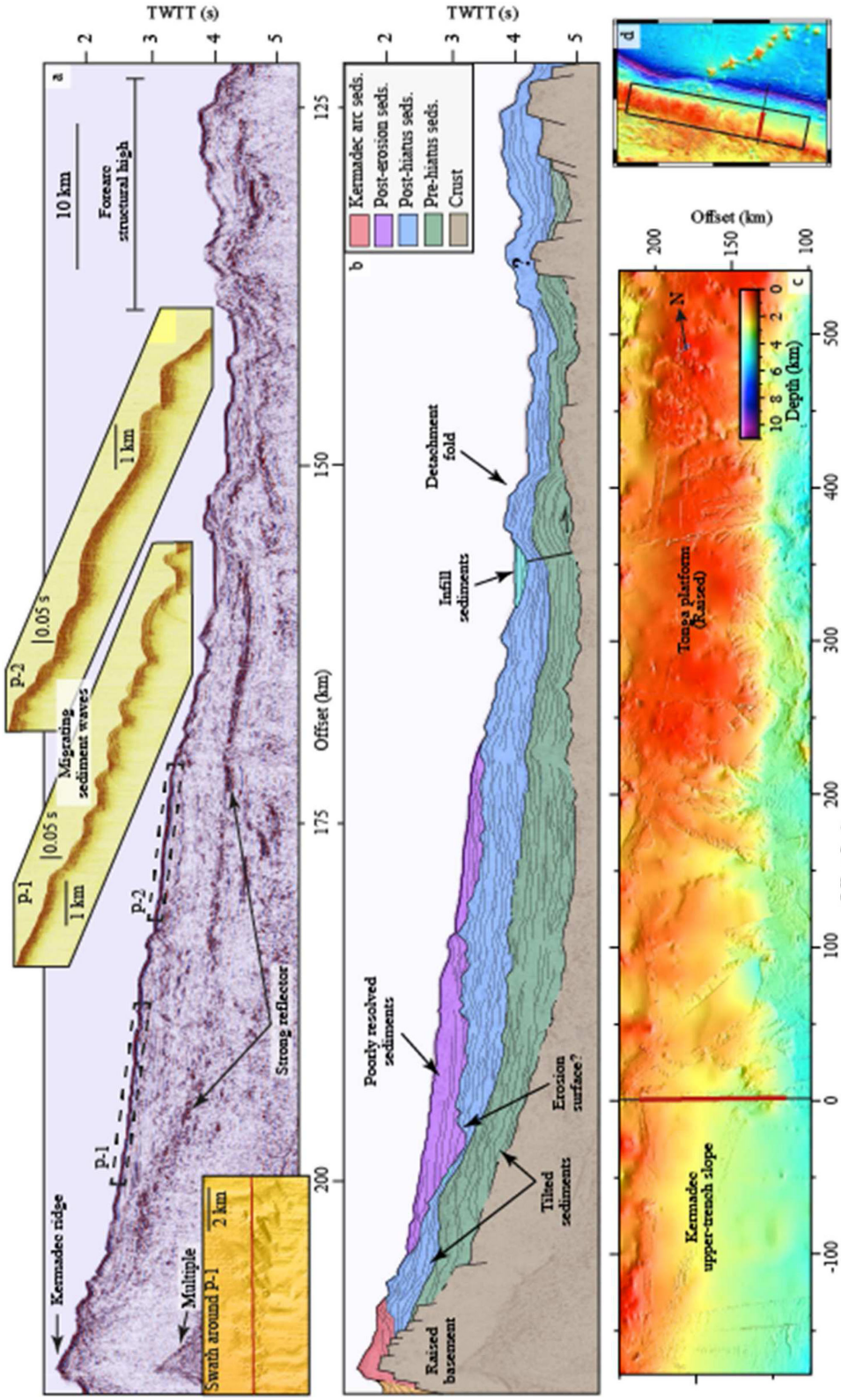

Figure 5. (a) Annotated seismic reflection image of the Kermadec forearc structural high, upper-trench slope and arc. An arrow highlights the onset of the water column multiple on the section. Two Parasound sections, P-1 and P-2, and a magnified region of swath bathymetry data are inset to indicate the migrating sediment waves observed in the shallow subsurface. (b) Interpreted seismic section. The different sedimentary seismostratigraphic units indicated in the section and inset key represent sequences that are separated by depositional hiatuses and erosional surfaces. (c) Swath bathymetry map, centred on the upper-trench slope of the Tonga-Kermadec subduction system, highlights variations between background and raised forearc structure. (d) Extent of the bathymetry and MCS data (black box and red line, respectively) displayed in this figure, shown relative to the study area.

Downloaded from http://gji.oxfordjournals.org/ at Durham University Library on September 30, 2014

that the crust here is more structurally robust than in surrounding areas of the forearc.

Characteristically similar to the upper-trench slope of the Tonga forearc, the eastern slope of the structural high is observed for over 2000 km to the north of Profile D in a number of seismic reflection and refraction surveys (e.g. Karig 1970; Lonsdale 1986; Contreras-Reyes *et al.* 2011; Stratford *et al.* 2014), swath and global bathymetry data (Figs 4c and 5c), and in backscatter profiles (e.g. MacLeod & Lothian 1994). Contreras-Reyes *et al.* (2011) propose that this slope is a scarp; a surface representation of a crustal-scale, trenchward-dipping listric fault defined by a zone of low seismic velocity in the overriding plate. Although Profile D demonstrates that this slope is undergoing extension, there is no direct evidence of a listric fault causing the collapse of the mid-trench slope. The forearc structural high on Profile D, which is bathymetrically uplifted relative to the trench slopes and forearc basin, terminates and remains absent from the bathymetry data beyond ~10 km south of Profile D. To the north of the profile, this bathymetric rise merges with the elevated forearc basin of the Tonga Platform. Although differences in forearc structure may be expected between regions that are subjected to varying rates of subduction erosion (e.g. von Huene & Scholl 1991; Clift & Vannucchi 2004), the forearc high is observed for over 250 km to the south of the current LRSC collision zone (Figs 4 and 5). The mid-trench slope scarp is significantly less prominent south of the LRSC collision, as adjacent basins are vertically offset by up to 1.5 km south of ~26°S compared to consistent offsets of ~3 km to the north (Lonsdale 1986; MacLeod & Lothian 1994; Clift *et al.* 1998; Contreras-Reyes *et al.* 2011). Such substantial discrepancies in the vertical offset along this scarp suggest that the forces involved in generating this feature have either been on-going for a longer period of time, or are of a much greater magnitude, north of the LRSC collision. The presence of this mid-trench slope and structural high, traversing ~100 km into the background region of the Kermadec subduction system despite being less prominent, suggests a link to an underlying forearc structural and deformational trend, or to the lateral propagation of forearc uplift caused by LRSC indentation.

4.6 Upper-trench slope

The upper-trench slope gently rises from the western edge of the forearc structural high to the Kermadec arc (Fig. 5). Thick sedimentary successions of up to 2 s TWTT, which are divided into two units by a strong reflection event (located along the pre- and post-hiatus seismostratigraphic boundary in Fig. 5b), comprise the fill of a forearc basin on the upper-trench slope. The high amplitude reflection event, which is more prominent than the reflection event associated with the top of the basement (Fig. 5b—McDougall 1994), is observed consistently along the Kermadec subduction system (e.g. Karig 1970; Gillies & Davey 1986). Parson *et al.* (1992) and Clift *et al.* (1994) record a depositional hiatus from 32 to 16 Ma that could have enabled the consolidation and diagenesis of sediments across the forearc and thus, by establishing a density contrast with subsequently deposited sediments, be capable of generating the observed high-amplitude reflection event. While other causes of this contrast are plausible, none are observed in the borehole data to an extent that could have generated the amplitude of this reflection.

Reflections from the upper-trench slope are rarely observed for more than 10 km along-profile, but do show onlap onto the basement and older parts of the sedimentary succession in places. These observations suggest that sediments on the slope were deposited by temporally distinct events that originated higher up the forearc (Fig. 5b). Parasound data, which effectively image the shallow subsurface where the MCS profile only images transparent or chaotic units on the upper-trench slope along Profile D, and swath bathymetry data indicate the presence of migrating sediment waves on the forearc basin (Fig. 5a insets). Gillies & Davey (1986) propose that gravity dominated flows initiated on the forearc high deposit volcaniclastic material as turbidites along the upper-trench slope further south. Although no sediment cores are available for the Kermadec upper-trench slope, ODP hole 840 confirms the dominance of turbidite deposits on the Tonga forearc to the north (Parson *et al.* 1992; Clift 1994; Clift *et al.* 1994). The lack of boreholes and cores from the Kermadec upper-trench slope, and the ambiguity of whether migrating waves observed in Parasound data are formed by downslope (turbidite) or along-slope (contourite) flows (Damuth 1979, 1980; Flood 1980), results in an inconclusive interpretation. However, the migrating waves are evidence of prevalent underwater currents and significant sediment reworking in the Kermadec forearc basin.

Although laterally variable, reflectors on the forearc high are broadly similar (Fig. 5a). They are concordant with the concave-up structure of the forearc crust, exhibiting dominant dip in the direction of the trench (Karig 1970). Dip angle increases with depth through the succession and suggests that the sediments, which begin to deposit as the gradient of the slope reduces, have been progressively rotated trenchward since their emplacement (Clift *et al.* 1994). These tilted sequences are only present within the westernmost 30 km of the upper trench slope and are particularly prominent over the region of faulted basement immediately east of the Kermadec arc. Thus, uplift of the arc relative to the adjacent slopes, rather than the trenchward rotation of the entire forearc, appears to be the primary mechanism for the adjustment of sediment dip.

The upper-trench slope bathymetry along Profile D resembles that observed for almost 200 km to the south (Fig. 5c) and that described by Karig (1970). As such, it is clear that the upper-trench slope and associated forearc basin along Profile D can be considered as the background structure and, thus, is undeformed by LRSC collision. Swath data for the region up to 30 km to the north indicates that the forearc basin structure progressively changes; decreasing in water depth to more closely reflect the Tonga Ridge geometry (e.g. Contreras-Reyes *et al.* 2011; Stratford *et al.* 2014). Deformation of the forearc in this region is constrained to ~50 km closer to present-day indentation of the LRSC than was observed in the mid-trench slope. This either suggests that the influence of the LRSC collision on the different structural blocks varies laterally, or supports the hypothesis that a pre-existing structural feature may be influencing forearc deformation regardless of the effects of the LRSC subduction.

4.7 Kermadec arc

The Kermadec arc corresponds to the shallowest part of the Kermadec trench–forearc–backarc system at 1.5 s TWTT water depth (~1100 m—Fig. 6). Sediments overlying arc basement are poorly resolved by the MCS data, with the only observable reflection events located on the slope to the east of the ridge (represented by line drawings of the Kermadec arc sediments in Figs 5b and 6b). These sedimentary reflectors terminate against the seabed and are discordant with the westernmost trenchward-dipping units of the upper-trench slope. Strong bottom currents that transport material along the strike of the ridge may have deposited these westward-dipping

Downloaded from http://gji.oxfordjournals.org/ at Durham University Library on September 30, 2014

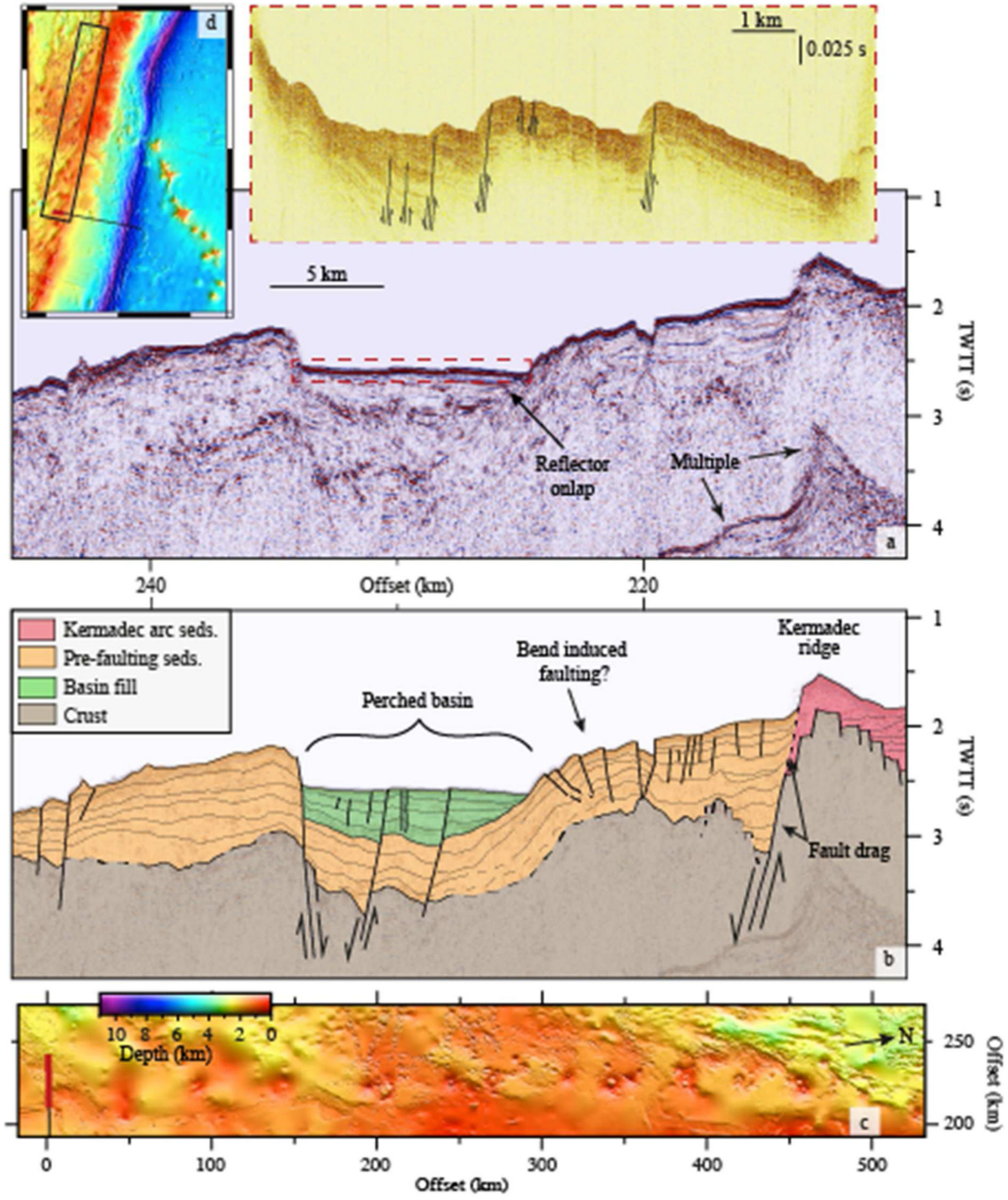

Figure 6. (a) Seismic section across the Kermadec arc and slope into the backarc. The water column multiple is indicated by arrows, and the red-dashed box shows the extent of the inset Parasound data, which images up to ~75 m of basin infill. Note the apparent lack of reflections above the basement of the Kermadec arc. (b) Annotated interpretation of (a), with inset key indicating the different seismostratigraphic units displayed. (c) Swath bathymetry data along the Kermadec and Tonga arcs. (d) Extent of the bathymetry and MCS data (black box and red line, respectively) displayed in this figure, shown relative to the study area.

sediments and caused their subsequent erosion. This suggests that the depositional and erosive regimes across the Kermadec arc are laterally and temporally variable (e.g. Gillies & Davey 1986).

Sediments on the backarc slope onlap against the ~1.3 s TWTT offset normal fault that bounds the western edge of the Kermadec arc (see Fig. 6b). There is a set of small normal faults (each being 0.1–0.2 s TWTT in offset), antithetic to the main fault, which enables the thickness of the sediment deposits to increase with proximity to the major offset. The sedimentary reflections at the base of the fault are much less pronounced which indicates that they may be more deformed than those at the top. Together, these observations imply that this major extensional fault has progressively developed following the initiation of deposition in the region.

Uplift or reduced subsidence of the arc, relative to both the upper-trench slope and the backarc, suggests that the Kermadec arc is underlain by relatively thick, buoyant crust. This structurally high region may be underlain by a thick low velocity basement, such as that observed ~270 km north of Profile D beneath the Tonga

Downloaded from http://gji.oxfordjournals.org/ at Durham University Library on September 30, 2014

arc (Stratford *et al.* 2014). Similar subarc basement structure is to be expected of the Tonga and Kermadec arcs, as the inception of present-day volcanic activity is thought to have occurred simultaneously along both arcs in response to minor changes in plate motion between 28 and 24 Ma (Lonsdale 1988; Ballance *et al.* 1999).

4.8 Backarc slope

In the backarc region west of the Kermadec arc, the seabed begins to increase in depth. Sediments are on average ~0.6 s TWTT thick, and the basement reflector remains roughly concordant with the seabed (Fig. 6b). A perched basin, observed in both the MCS and swath bathymetry data, lies between 10 and 20 km west of the forearc high. This basin terminates to the west against a large (>0.5 s TWTT offset) eastward-dipping normal fault that crosscuts the basement and pre-existing sediments. At the eastern end of the perched basin, lower resolution imaging of the basement results in the inference of a broad rollover anticlinal structure, which most likely caused the radial normal faults (<0.05 s TWTT offset) observed in the overlying sediments.

Following the generation of the main eastward-dipping fault, infill of this perched basin reaches 0.4 s TWTT thick (Figs 6a and b). Onlap of both the pre-existing and infill sediments against this major offset suggests continual displacement, and thus reactivation of the fault. Two antithetic normal faults, which appear to cause a clockwise rotation of the basement and overlying sediments, further divide the basin infill and surface, and also indicate recent activation. Smaller-scale faults (<0.01 s TWTT offset) are evident in the Parasound data and accommodate the extensional stress field that this rotation generates (Fig. 6a inset). The Parasound profile through the basin also indicates that infill has occurred in a series of fault-dependent stages, with deposition effectively working to remove any bathymetric variations.

The many scales and prevalence of normal faulting observed west of the Kermadec arc indicate that this region is being continually extended. These extensional forces may be associated with extension of the backarc (Delteil *et al.* 2002) or the oblique subduction angle of the Pacific Plate and LRSC (Pelletier & Louat 1989; Bonnardot *et al.* 2007). Although the active centre of the backarc rift is located >150 km west of the Kermadec arc at this latitude, and is thus unlikely to be inducing any measurable extension at present, the opening of the Havre Trough ~5 Ma most likely reactivated existing faults over a broad region (Delteil *et al.* 2002). Pelletier & Louat (1989) and Bonnardot *et al.* (2007) note the focal mechanisms of local shallow (<70 km) seismicity that indicate trench-perpendicular extension, just north of the backarc along Profile D. Despite swath bathymetry data being sparse for ~50 km south and north of the profile, it is expected that the observed trench-parallel extension is present throughout this region. In comparison, swath bathymetry data further north in the Tonga arc indicates a series of left-stepping extensional basins (Pelletier & Louat 1989). These most likely formed in response to the general extension of the backarc, and have since been pulled apart by the trench-parallel, strike-slip motion induced by oblique subduction (Delteil *et al.* 2002; Bonnardot *et al.* 2007).

4.9 Summary of the structural evolution of the Kermadec forearc

Since the initiation of Pacific Plate subduction in the middle Eocene, the sedimentary and structural configuration of the Kermadec forearc has evolved into the system present today. Although Profile D only images a 2-D transect through this complex system, a detailed analysis of the observed sedimentary units, and their relationships with different structures, enables the evolution of the forearc to be interpreted. The lack of borehole data in the region prevents the use of date constraints in understanding this evolution; however, distinct stages of forearc development can be considered relative to one another to gain a greater insight into major structural changes. Fig. 7 summarizes the structural and stratigraphic evolution of the Kermadec forearc along Profile D in four stages based on previous studies and the interpretation of the MCS and swath bathymetry data presented in this paper.

As subduction initiated along the Tonga-Kermadec trench ~44 Ma, the forearc raised by ~1 km and the trench depressed to its current depth (Parson *et al.* 1992; Bloomer *et al.* 1995). After the initiation of subduction, the forearc evolved through the following stages (see Fig. 7):

Stage 1

(i) Uplift of the Kermadec arc begins (Ballance *et al.* 1989).

(ii) Volcanic material is generated along the arc and distributed to the surrounding basins (Clift 1994).

(iii) The forearc and backarc basins subside relative to the Kermadec arc.

(iv) Subduction causes basal subduction erosion and subsequent forearc extension (e.g. von Huene *et al.* 2004), promoting fracturing and faulting of the lower- and mid-trench slopes (Contreras-Reyes *et al.* 2011).

Stage 2

(i) The backarc slope continues to be downthrown relative to the arc enabling further sedimentation.

(ii) Volcaniclastic material accumulates on the trench slope-basins before the onset of a depositional hiatus from ~32 Ma (Clift *et al.* 1994).

(iii) The active landward-dipping normal fault of the mid-trench slope migrates eastward (to fault 1—Fig. 7), as extension of the forearc slopes continues.

(iv) Extension of the mid- and upper-trench slopes causes them to subside; the region between these basins is more structurally robust, and is therefore effectively uplifted.

Stage 3

(i) Extension of the backarc, possibly related to opening of the Havre Trough ~5 Ma (Delteil *et al.* 2002), produces a seaward normal fault and a perched basin west of the Kermadec arc.

(ii) Volcaniclastic material continues to be generated and deposited on the trench slopes from ~16 Ma (Clift *et al.* 1994) until ~5 Ma (Delteil *et al.* 2002).

(iii) Extension and subsidence of the mid- and upper- trench slopes increases along pre-existing faults, for example fault 1, and new faults around the forearc structural high.

Stage 4 (Present day)

(i) The backarc perched basin begins to be infilled by volcaniclastic material.

(ii) Deposition of sediments on the upper-trench slope resumes following a period of erosion.

(iii) Deposits on the forearc structural high are eroded and deposited on the mid-trench slope basin.

(iv) A reversal in the offset across fault 1 (Fig. 7) and the eastward migration of the active landward-dipping fault, to fault 2 (Fig. 7), on the mid-trench slope generates a new basin.

Downloaded from http://gji.oxfordjournals.org/ at Durham University Library on September 30, 2014

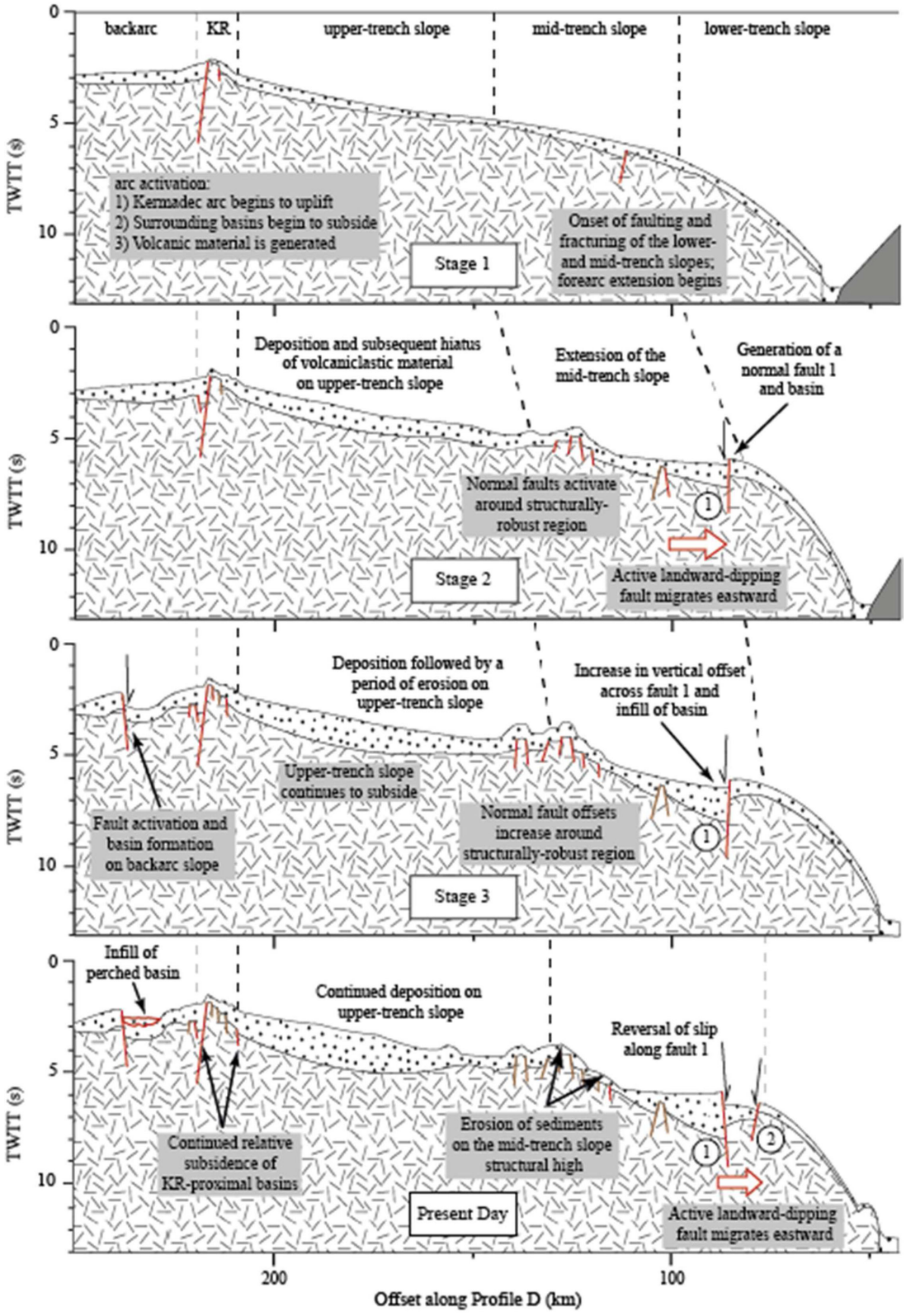

Figure 7. A series of schematic diagrams representing the proposed evolution of the Kermadec forearc along Profile D, based on previous studies and the interpretation of the MCS and swath bathymetry data presented in Figs 3–6. Stages 1–4 define key periods of forearc development, focussing on major structural and stratigraphic changes, with Stage 4 being a simplified model of the present-day forearc structure. The different stages are loosely defined spatially and temporally due to a lack of constraint from borehole data. The background mesh indicates the major forearc structural units: the lower-, mid- and upper-trench slopes, the Kermadec ridge (KR), and the backarc.

Downloaded from http://gji.oxfordjournals.org/ at Durham University Library on September 30, 2014

5 REGIONAL CHANGES IN FOREARC STRUCTURE

The trench-parallel variations in the structural units of the Kermadec trench–forearc–backarc system are inherently related and, as such, form coherent blocks observable in regional scale bathymetry and satellite-derived free-air gravity anomaly maps (Figs 8a and b, respectively—Sandwell & Smith 2009). Perhaps the biggest influence on the development of these blocks is the structure and erosive nature of the downgoing plate, and the mechanical strength of the overriding plate (von Huene & Scholl 1991; Clift & Vannucchi 2004; von Huene *et al.* 2004). Fig. 8(a) shows that the bathymetry (upper surface) of the Pacific oceanic plate is generally smooth, except where the LRSC seamounts protrude up to 3 km from the seabed (Watts *et al.* 1988) and in the vicinity of the Tonga-Kermadec trench, where the plate bends and is faulted prior to subduction (Lonsdale 1986; Aubouin 1989). Although the flexural moat surrounding the LRSC is not apparent in the bathymetry data, the free-air gravity anomaly map indicates a region of up to 30 mGal lower anomaly amplitude relative to the background oceanic plate surrounding the seamount chain (Fig. 8b). This >100-km-wide region corresponds to the lateral extent of the magma-intruded crust, deeper crust–mantle boundary, and up to 1.6-km-thick sediment-filled moat constrained by wide-angle seismic refraction data (Contreras-Reyes *et al.* 2010). The southern boundary of this loaded region of oceanic lithosphere coincides with shallowing of the Kermadec trench ∼150 km to the south of the LRSC collision (Fig. 3c). The free-air gravity anomaly also highlights the presence of the Osbourn spreading centre (OSC in Figs 8a and b) as an east–west trending linear feature just north of the LRSC collision zone at ∼26°S (Billen & Stock 2000).

Comparison of a series of trench–forearc–backarc profiles (Profiles 1–5—Fig. 8) extracted from the bathymetry and free-air gravity anomaly maps (Figs 8a and b, respectively) clearly shows the along-strike extent of the major structural units of the Tonga-Kermadec subduction system. A 200 mGal negative anomaly region immediately west of the Tonga-Kermadec trench approximately defines the lower- and mid-trench slopes of their forearcs, except in the vicinity of the LRSC collision where gravity anomaly values only reach –100 mGal. This gravity anomaly across the lower- and mid-trench slopes is most likely caused by the simple bathymetric gradient across the forearc, although the higher amplitude anomaly present in the LRSC collision zone may be indicative of a currently subducting seamount (e.g. Timm *et al.* 2013).

Further west, south of 28°S, a gravity anomaly of 0–50 mGal marks the upper-trench slope of the background Kermadec forearc. The bathymetry of this region displays a marked change in geometry from being slightly concave in the south (Profiles 1 and 2—Karig 1970), through a transition from Profile 2 (which is coincident with Profile D) to just north of Profile 3, where the forearc is elevated by ∼3 km and convex in shape (associated with a >100 mGal gravity anomaly), typical of the Tonga forearc basin (Profile 5). With such a clear change in forearc geometry over this region, it might be inferred that there are significant variations in sedimentary thickness as well as the crustal structure of the overriding plate (e.g. Ballance *et al.* 1989). However, the maps and profiles demonstrate that the relationship between the free-air gravity anomaly and bathymetry vary little across these zones, except at the southern end of the transitional region between the Kermadec upper-trench slope and the Tonga Platform. Interestingly, this anomalously high gravity anomaly (>100 mGal) in the transitional zone, which is intersected at its southern extent by Profile 2, coincides with the inferred structurally robust forearc high observed along Profile D. The positive gravity anomaly here suggests that the structurally robust crust between the mid- and upper-trench slopes of the Kermadec forearc is of a higher density than in surrounding regions, and thus may represent a remnant of the old Eocene arc (Bloomer *et al.* 1995; Collot & Davy 1998).

The transitional zone between the background forearc (geometrically concave—green region in Fig. 8c) and highly deformed and elevated Tonga Platform (geometrically convex—red and blue regions in Fig. 8c) is currently only being directly influenced by background Pacific Plate subduction. Despite the inference of a dense and robust remnant crust underlying the Kermadec structural high, deformation around this region along Profile D (Profile 2 in Fig. 8) appears to be on-going and of a greater magnitude than that observed further south. As a result, this transitional feature appears to be generated by not only an older structural trend, but also by diffuse uplift of the Kermadec forearc caused by the collision of the LRSC up to 250 km to the north (Parson *et al.* 1992; Collot & Davy 1998).

6 CONCLUSIONS

Despite being unable to image below the top of the basement, the MCS and Parasound data acquired along Profile D traversing the Kermadec trench and forearc, has enabled the structure and stratigraphy of the underthrusting (downgoing) and overriding plates to be determined. By synthesising this information with relatively sparse shipboard swath bathymetry data sets and satellite-derived bathymetry and free-air gravity data, we have been able to relate the observed along-profile characteristics with trench-parallel variations in background features and underlying subduction processes. We conclude that:

1. The subducting plate is characterized by large-offset normal faults, which form horst and graben structures up to 2 km deep, 15 km across and >200 km in trench-parallel length. Fault offsets grow with proximity to the trench, as extensional stresses increase with bending of the downgoing plate.
2. Although the subducting Pacific Plate is poorly sedimented prior to entering the trench (<100 m), trench infill at ∼28°S is significantly thicker than expected, exceeding 1 km. This increase most likely results from increased input of forearc-derived volcaniclastic sediments and the redistribution of sediments along-trench by an inferred southward-flowing current.
3. Subduction of the highly faulted Pacific Plate persistently erodes the basal and frontal sections of the overriding plate, causing continual extension and collapse of the ∼70-km-wide lower- and mid-trench slopes. Although this steady-state rate of erosion is thought to be below 1.5 km Myr^{-1} (Clift & MacLeod 1999), the effect is observed in the pervasive normal faulting of the mid-trench slope as it gradually subsides and collapses into the trench together with the lower-trench slope.
4. Striking variations in along-arc bathymetric geometry and the presence of a free-air gravity anomaly high between the mid- and upper-trench slopes, suggests that a region of higher density and structurally robust crust sits beneath the forearc structural high.
5. Proximal to the southern end of the LRSC collision with the Kermadec trench, there is an ∼70 km wide concave forearc basin on the upper-trench slope, and the arc forms a single pronounced ridge. The forearc and backarc slopes are covered by accumulations of locally derived volcaniclastic sediments, with migrating

Downloaded from http://gji.oxfordjournals.org/ at Durham University Library on September 30, 2014

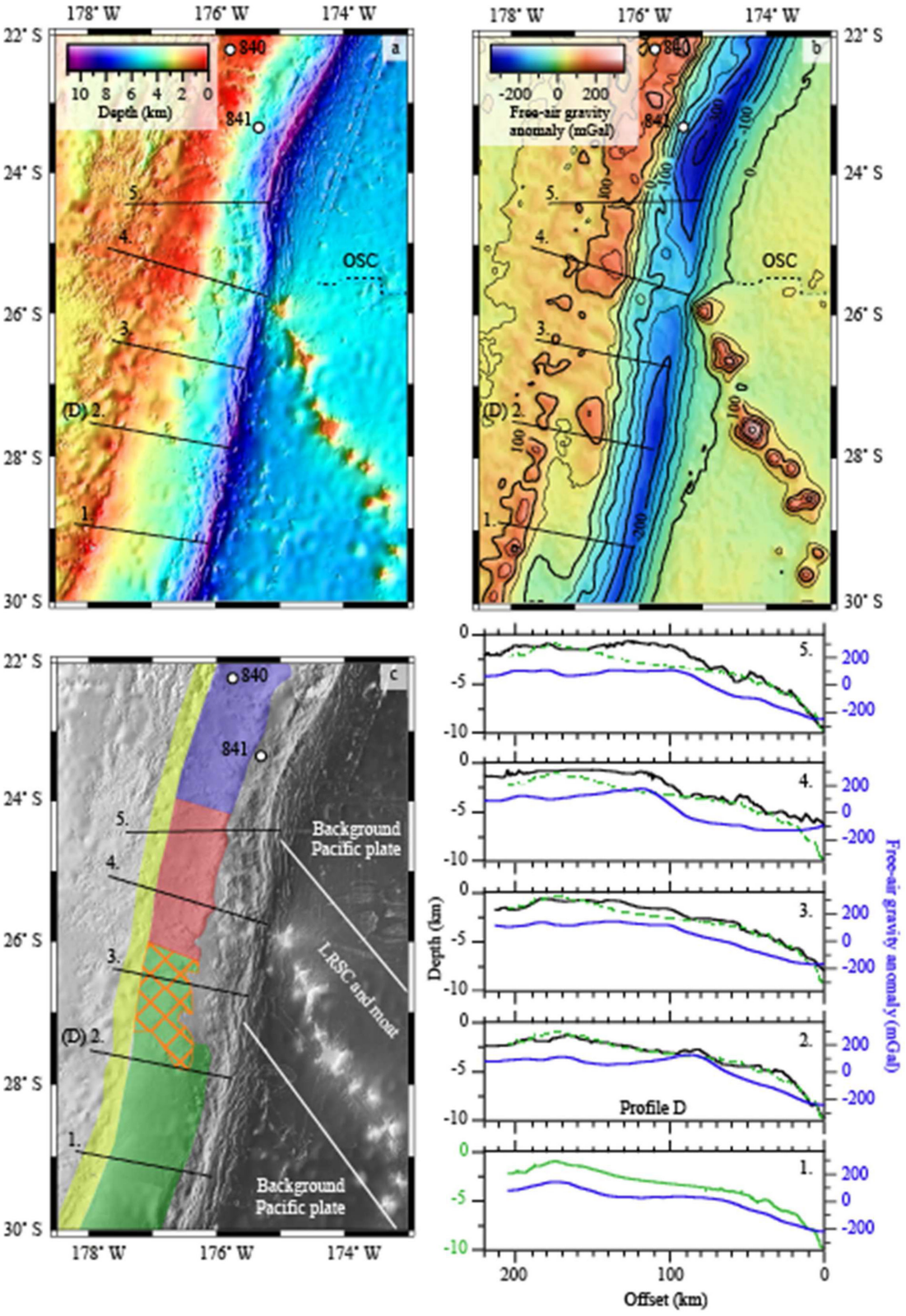

Figure 8. (a) Bathymetry and (b) satellite-derived free-air gravity anomaly maps of the Tonga-Kermadec study region. A dashed black line indicates the location of the Osbourn Spreading Centre (OSC). Profiles 1–5 were selected to sample the Kermadec forearc, where swath bathymetry data has been acquired, whilst being separated by a relatively consistent offset. Profile 2 is coincident with Profile D. The free-air gravity anomaly map highlights the presence of the LRSC and moat on the subducting plate, and indicates distinct variations between the pre-, current- and post-collision zones. These different zones are outlined in (c) by the green, red and blue boxes, respectively. The yellow region represents the volcanic arc, and the orange cross-hachured box over the pre-collision zone delimits the region of transitional deformation. To the right of (c), profiles of bathymetry (black lines, with blue lines representing normal Kermadec forearc structure along Profile 1 for comparison) and the free-air gravity anomaly (blue lines) show the along-forearc changes in structure and deformation.

Downloaded from http://gji.oxfordjournals.org/ at Durham University Library on September 30, 2014

sediment waves suggesting that reworking of these deposits by arc-parallel and downslope currents is likely. At least two periods of non-deposition and erosion are recorded in the MCS data.

6. Perhaps the most significant observation, however, is the raising and broadening of the forearc basin immediately north of Profile D. Heading further north, this region develops into the shallow and wide Tonga Platform over a distance of 250 km, suggesting that an underlying structural trend may be present, and that LRSC subduction deforms a wider region of the forearc than its actual footprint on the subducting plate.

ACKNOWLEDGEMENTS

We would like to thank all those involved in the data acquisition for the *R/V Sonne* cruise SO215, including the captain, crew and seagoing technicians from the U.K.'s Natural Environment Research Council (NERC) National Marine Facility Sea Systems and Exploration Electronics Ltd. We are grateful to the two anonymous reviewers for their thoughtful and helpful comments on this paper. The MCS data were processed and plotted using Claritas™. All other figures were generated with the Generic Mapping Tools (Wessel & Smith 1998). This research was funded by the NERC (grant reference NE/F004273/1) in collaboration with the TOTAL project (Peirce & Watts 2011). All data from cruise SO215 are archived at the NERC's British Oceanographic Data Centre (BODC), and the final submitted version of this manuscript is available through Durham Research Online (dro.dur.ac.uk).

REFERENCES

Aubouin, J., 1989. Some aspects of the tectonics of subduction zones, *Tectonophysics,* **160,** 1–21.

Ballance, P.F., Scholl, D.W., Vallier, T.L., Stevenson, A.J., Ryan, H. & Herzer, R.H., 1989. Subduction of a late Cretaceous seamount of the Louisville Ridge at the Tonga Trench: a model of normal and accelerated tectonic erosion, *Tectonics,* **8,** 953–962.

Ballance, P.F., Ablaev, A.G., Pushchin, I.K., Pletnev, S.P., Birylina, M.G., Itaya, T., Follas, H.A. & Gibson, G.W., 1999. Morphology and history of the Kermadec trench-arc-backarc basin-remnant arc system at 30 to 32°S: geophysical profile, microfossil and K-Ar data, *Mar. Geol.,* **159,** 35–62.

Bevis, M. *et al.*, 1995. Geodetic observations of very rapid convergence and back-arc extension at the Tonga arc, *Nature,* **374,** 249–251.

Billen, M. & Stock, J., 2000. Morphology and origin of the Osbourn Trough, *J. geophys. Res.,* **105,** 481–489.

Billen, M., Cowgill, E. & Buer, E., 2007. Determination of fault friction from reactivation of abyssal-hill faults in subduction zones, *Geology,* **35,** 819–822.

Bloomer, S.H., Taylor, B., MacLeod, C.J., Stern, R.J., Fryer, P. & Johnson, L., 1995. Early arc volcanism and the ophiolite problem: a perspective from drilling in the western Pacific, in *Active Margins and Marginal Basins: A Synthesis of Ocean Drilling in the Western Pacific,* American Geophysical Union Monograph 88, pp. 1–30, eds Taylor, B. & Natland, J.H., American Geophysical Union.

Bonnardot, M.-A., Régnier, M., Ruellan, E., Christova, C. & Tric, E., 2007. Seismicity and state of stress within the overriding plate of the Tonga-Kermadec subduction zone, *Tectonics,* **26,** TC5017, doi:10.1029/2006TC002044.

Bouma, A.H., 1962. *Sedimentology of Some Flysch Deposits: A Graphic Approach to Facies Interpretation,* Elsevier.

Brodie, J.W. & Hatherton, T., 1958. The morphology of Kermadec and Hikurangi trenches, *Deep-Sea Res.,* **5,** 18–28.

Burns, R.E., Andrews, J.E. & van der Lingen, G.J., 1973. Site 204 Initial Report, in *Proceedings of the Ocean Drilling Program, 21,* College Station, Texas, Ocean Drilling Program, pp. 33–56.

Caldwell, J.G., Haxby, W.F., Karig, D.E. & Turcotte, D.L., 1976. Observations of flexure and the state of stress in the oceanic lithosphere, *Earth planet. Sci. Lett.,* **31,** 239–246.

Caress, D.W. & Chayes, D.N., 1996. Improved processing of Hydrosweep data on the R/V Maurice Ewing, *Mar. geophys. Res.,* **18,** 631–650.

Castillo, P.R., Lonsdale, P.F., Moran, C.L. & Hawkins, J.W., 2009. Geochemistry of mid-Cretaceous Pacific crust being subducted along the Tonga-Kermadec Trench: implications for the generation of arc lavas, *Lithos,* **112,** 87–102.

Clift, P.D., 1994. Controls on the sedimentary and subsidence history of an active plate margin: an example from the Tonga Arc (southwest Pacific), in *Proceedings of the Ocean Drilling Program,* Scientific Results, College Station, TX (Ocean Drilling Program), Vol. 135, pp. 173–188.

Clift, P.D. & MacLeod, C.J., 1999. Slow rates of subduction erosion estimated from subsidence and tilting of the Tonga forearc, *Geology,* **27,** 411–414.

Clift, P.D. & Vannucchi, P. 2004, Controls on tectonic accretion versus erosion in subduction zones: implications for the origin and recycling of the continental crust, *Rev. Geophys.,* **42,** RG2001, doi:10.1029/2003RG000127.

Clift, P.D., Bednarz, U., Bøe, R., Rothwell, G., Hodkinson, R.A., Ledbetter, J.K., Pratt, C.E. & Soakai, S., 1994. Sedimentation on the Tonga forearc related to arc rifting, subduction, erosion, and ridge collision: A synthesis of results from sites 840 and 841, in *Proceedings of the Ocean Drilling Program,* Scientific Results, College Station, TX (Ocean Drilling Program), Vol. 135, pp. 843–855.

Clift, P.D., MacLeod, C.J., Tappin, D.R., Wright, D.J. & Bloomer, S.H., 1998. Tectonic controls on sedimentation and diagenesis in the Tonga Trench and forearc, southwest Pacific, *Bull. geol. Soc. Am.,* **110,** 483–496.

Collot, J.-Y. & Davy., 1998. Forearc structures and tectonic regimes at the oblique subduction zone between the Hikurangi Plateau and the southern Kermadec margin, *J. geophys. Res.,* **103,** 623–650.

Contreras-Reyes, E., Grevemeyer, I., Watts, A.B., Planert, L., Flueh, E.R. & Peirce, C., 2010. Crustal intrusion beneath the Louisville hotspot track, *Earth planet. Sci. Lett.,* **289,** 323–333.

Contreras-Reyes, E., Grevemeyer, I., Watts, A.B., Flueh, E.R., Peirce, C., Moeller, S. & Papenberg, C., 2011. Deep seismic structure of the Tonga subduction zone: implications for mantle hydration, tectonic erosion, and arc magmatism, *J. geophys. Res.,* **116,** B10103, doi:10.1029/2011JB008434.

Damuth, J.E., 1979. Migrating sediment waves created by turbidity currents in the northern South China Basin, *Geology,* **7,** 520–523.

Damuth, J.E., 1980. Use of high-frequency (3.5–12 kHz) echograms in the study of near-bottom sedimentation processes in the deep-sea: a review, *Mar. Geol.,* **38,** 51–75.

Davy, B., 1992. The influence of subducting plate buoyancy on subduction of the Hikurang-Chatham Plateau beneath North Island, New Zealnad, in *Geology and Geophysics of Continental Margins,* Vol. 53, pp. 75–91, eds Watkins, J.S., Zhiqiang, F. & McMillen, K.J., AAPG Mem.

Davy, B. & Collot, J.-Y., 2000. The Rapuhia Scarp (northern Hikurangi Plateau)—its nature and subduction effects on the Kermadec Trench, *Tectonophysics,* **328,** 269–295.

Delteil, J., Ruellan, E., Wright, I. & Matsumoto, T., 2002. Structure and structural development of the Havre Trough (SW Pacific), *J. geophys. Res.,* **107,** doi:10.1029/2001JB000494.

Dickinson, W.R. & Seely, D.R., 1979. Structure and stratigraphy of forearc regions, *Am. Assoc. Petrol. Geol. Bull.,* **63,** 2–31.

Flood, R.D., 1980. Deep-sea sedimentary morphology: modelling and interpretation of echo-sounding profiles, *Mar. Geol.,* **38,** 77–92.

Gillies, P.N. & Davey, F.J., 1986. Seismic reflection and refraction studies of the Raukumara forearc basin, New Zealand, *N. Z. J. Geol. Geophys.,* **29,** 391–403.

Grevemeyer, I. & Flüh, E., 2008. FS Sonne SO195 cruise report: TOnga thrust earthquake asperity at Louisville ridge (TOTAL), pp 101.

Grevemeyer, I., Kaul, N., Diaz-Naveas, J.L., Villinger, H.W., Ranero, C.R. & Reichert, C., 2005. Heat flow and bending-related faulting at subduction trenches: case studies offshore of Nicaragua and central Chile, *Earth planet. Sci. Lett.,* **236**(1–2), 238–248.

Downloaded from http://gji.oxfordjournals.org/ at Durham University Library on September 30, 2014

Habermann, R.E., McCann, W.R. & Perin, B., 1986. Spatial seismicity variations along convergent plate boundaries, *Geophys. J. R. astr. Soc.,* **85,** 43–68.

Hawkins, J.W., Bloomer, S.H., Evans, C.A. & Melchior, J.T., 1984. Evolution of intra-oceanic arc-trench systems, *Tectonophysics,* **102,** 175–205.

Herzer, R.H. & Scholl, D.W. Scientific Staff, 1984. Initial report on 1984 R/V S.P. Lee cruise L3–84-SP: Tonga Ridge, Lau Ridge, and Lau Basin, SOPAC Cruise Report No. 93, pp. 8.

Intergovernmental Oceanographic Commission (IOC), International Hydrographic Organization (IHO), and British Oceanographic Data Centre (BODC), 2003. *Centenary Edition of the General Bathymetric Chart of the Oceans Digital Atlas*, Published on CDROM on Behalf of the IOC and the IHO as Part of the GEBCO; BODC, Liverpool.

Karig, D.E., 1970. Ridges and basins of the Tonga-Kermadec Island Arc system, *J. geophys. Res.,* **75,** 239–254.

Katz, H.R., 1981. Plate margin transition from oceanic arc-trench to continental system: the Kermadec-New Zealand example, *Tectonophysics,* **87,** 49–64.

Laursen, J., Scholl, D.W. & von Huene, R., 2002. Neotectonic deformation of the central Chile margin: Deepwater forearc basin formation in response to hot spot ridge and seamount subduction, *Tectonics,* **21**(5), 1–27.

Lewis, K.B., 1994. The 1500 km-long Hikurangi Channel: trench-axis channel that escapes its trench, crosses a plateau, and feeds a fan drift, *Geo-Mar. Lett.,* **14,** 19–28.

Lonsdale, P., 1986. A multibeam reconnaissance of the Tonga Trench axis and its intersection with the Louisville Guyot chain, *Mar. geophys. Res.,* **8,** 295–327.

Lonsdale, P., 1988. Geography and History of the Louisville Hotspot Chain in the Southwest Pacific, *J. geophys. Res.,* **93,** 3078–3104.

MacLeod, C.J., 1994. Structure of the outer Tonga forearc at site 841, in *Proceedings of the Ocean Drilling Program,* Scientific Results, College Station, TX (Ocean Drilling Program), Vol. 135, pp. 313–329.

MacLeod, C.J. & Lothian, A., 1994. Comparison of GLORIA sidescan sonar and core derived structural data from Site 841, Tonga Trench, in *Proceedings of the Ocean Drilling Program Scientific Results,* College Station, TX (Ocean Drilling Program), Vol. 135, pp. 373–382.

Maksymowicz, A., Conreras-Reyes, E., Grevemeyer, I. & Flueh, E., 2012. Structure and geodynamics of the post-collision zone between the Nazca-Antarctic spreading center and South America, *Earth planet. Sci. Lett.,* **345–348,** 27–37.

Malahoff, A., Feden, R.H. & Fleming, H.S., 1982. Magnetic anomalies and tectonic fabric of marginal basins north of New Zealand, *J. geophys. Res.,* **87,** 4109–4125.

McDougall, I., 1994. Data Report: Dating of rhyolitic glass in the Tongan forearc (hole 841B), in *Proceedings of Ocean Drilling Program Scientific Results,* College Station, TX (Ocean Drilling Program), Vol. 135, pp. 923–924.

Parson, L., Hawkins, J. & Allan, J., 1992. Site 840 Initial Report, in *Proceedings of the Ocean Drilling Program Scientific Results,* College Station, TX (Ocean Drilling Program), Vol. 135, pp. 313–329.

Peirce, C. & Watts, A.B., 2011. R/V Sonne SO215 Cruise Report, The Louisville Ridge-Tonga Trench collision: Implications for subduction zone dynamics, Unpublished, pp. 76.

Pelletier, B. & Dupont, J., 1990. Erosion, accretion, back-arc extension and slab length along the Kermadec subduction zone, Southwest Pacific, *Mar. Geol.,* **310,** 1657–1664.

Pelletier, B. & Louat, L., 1989. Seismotectonics and present-day relative plate motions in the Tonga-Lau and Kermadec-Havre region, *Tectonophysics,* **165,** 237–250.

Pontoise, B. *et al.* 1986. La subduction de la ride de Louisville le long de la fosse des Tonga: premiers resultats de la campagne SEAPSO (Leg V), *C. R. Acad. Sc. Paris,* **303**(10), 911–918.

Ranero, C.R., Phipps Morgan, J., McIntosh, K. & Reichert, C., 2003. Bending-related faulting and mantle serpentinization at the Middle America trench, *Nature,* **425,** 367–373.

Ranero, C.R., von Huene, R., Weinrebe, W. & Reichert, C., 2006. Tectonic processes along the Chile Convergent Margin, in *Frontiers in Earth Sciences,* Vol. 3: The Andes: Active Subduction Orogeny, pp. 91–121, eds Oncken, O. *et al.,* Springer.

Sandwell, D.T. & Smith, W.H.F., 2009. Global marine gravity from retracked Geosast and ERS-1 altimetry: ridge segmentation versus spreading rate, *J. geophys. Res.,* **114,** BO1411, doi:10.1029/2008JB006008.

Shreve, R.L. & Cloos, M., 1986. Dynamics of sediment subduction, melange formation, and prism accretion, *J. geophys. Res.,* **91**(B10), 10 229–10 245.

Stratford, W.A., Peirce, C., Funnell, M.J., Paulatto, M., Watts, A.B., Grevemeyer, I. & Basset, D., 2014. Louisville Ridge seamount subduction effects on forearc morphology and seismic structure of the Tonga-Kermadec subduction zone, *Geophys. J. Int.,* in press.

Sutherland, R., 1995. The Australia-Pacific boundary and Cenozoic plate motions in the SW Pacific: some constraints from Geosat data, *Tectonics,* **14,** 819–831.

Timm, C., Bassett, D., Graham, I.J., Leybourne, M.I., de Ronde, C.E.J., Woodhead, J., Layton-Matthews, D. & Watts, A.B., 2013. Louisville seamount subduction and its implication on mantle flow beneath the central Tonga-Kermadec arc, *Nature Commun.,* **4**(1720), doi:10.1038/ncomms2702.

von Huene, R. & Scholl, D.W., 1991. Observations at convergent margins concerning sediment subduction, subduction erosion, and the growth of continental crust, *Rev. Geophys.,* **29,** 279–316.

von Huene, R. & Ranero, C.R., 2003. Subduction erosion and basal friction along the sediment-starved convergent margin off Antofagasta, Chile, *J. geophys. Res.,* **108**(B2), doi:10.1029/2001JB001569pp.

von Huene, R., Corvalán, J., Flueh, E.R., Hinz, K., Korstgard, J., Ranero, C.R. & Weinrebe, W. the CONDOR Scientists, 1997. Tectonic control of the subducting Juan Fernández Ridge on the Andean margin near Valparaiso, Chile, *Tectonics,* **16**(3), 474–488.

von Huene, R., Ranero, C.R. & Vannucchi, P., 2004. Generic model of subduction erosion, *Geology,* **32,** 913–916.

Völker, D., Geersen, J., Contreras-Reyes, E. & Reichert, C., 2013. Sedimentary fill of the Chile Trench (32–46°): volumetric distribution and causal factors, *J. Geol. Soc., Lond.,* **79,** 723–736.

Watts, A.B., Bodine, J.H. & Steckler, M.S., 1980. Observations of flexure and the state of stress in the oceanic lithosphere, *J. geophys. Res.,* **85,** 6369–6376.

Watts, A.B., Weissel, J.K., Duncan, R.A. & Larson, R.L., 1988. Origin of the Louisville Ridge and its relationship to the Eltanin Fracture Zone system, *J. geophys. Res.,* **92,** 3051–3077.

Wessel, P. & Smith, W.H.F., 1998. New, improved version of the Generic Mapping Tools released, *EOS, Trans. Am. geophys. Un.,* **79,** 579, doi:10.1029/98EO00426.

Downloaded from http://gji.oxfordjournals.org/ at Durham University Library on September 30, 2014